EHE ($E \gtrsim 10^{20}\,\mathrm{eV}$) PARTICLES FROM TOP-DOWN PROCESSES

Pijush Bhattacharjee
Indian Inst. of Astrophysics
Bangalore

May 19, 2005

UHE05 miniprogram, KITP, Santa Barbara, May 2–20, 2005

- Why Top-Down (T-D)?
- General characteristics of T-D models of EHE particle production
- Benchmark requirements and general constraints on T-D models of EHECR
- Example: Cosmic strings as possible sources of EHE particles
- Particle Fluxes and detectability
- Conclusions

Why T-D?

There are strong indications of new physics beyond SM: E.g., small neutrino mass, $m_\nu \lesssim 0.1\,\mathrm{eV}$, may be explained by "see-saw" mechanism:

$$m_\nu \sim \frac{v_{\mathrm{EW}}^2}{M} \sim 0.1\,\mathrm{eV}\left(\frac{v_{\mathrm{EW}}}{100\,\mathrm{GeV}}\right)^2\left(\frac{10^{14}\,\mathrm{GeV}}{M}\right)\,\mathrm{eV}$$

$\Rightarrow$ New physics at high energy scales $M \gg M_{\mathrm{EW}}$.

– Physics beyond SM may allow massive "X" particles with $m_X > 10^{11}\,\mathrm{GeV}$.

– Decay of these X particles in the present epoch may give EHE particles with E up to m_X.

Two classes of Top-Down (T-D) models

- Decay of unstable X particles released from collapse/annihilation of cosmic Topological Defects (TDs) (e.g., cosmic strings, necklace, ...) formed during a symmetry-breaking phase transition in the early Universe at $T \gtrsim 10^{13}\,\mathrm{GeV}$.
- Decay of Long-lived Metastable Superheavy Relic Particles (MSRPs) with $\tau \gtrsim t_0$.

Spectra of observable particles in T-D models are fixed by particle physics (QCD, SUSY-QCD, ...) (no astrophysical acceleration) (but ?)
Generally predict:

- γ and ν rich spectra.
- Hard spectra ($\propto E^{-\alpha}$ with $\alpha < 2$) (but ?)

Top-Down "signal" vs. Bottom-up "background"

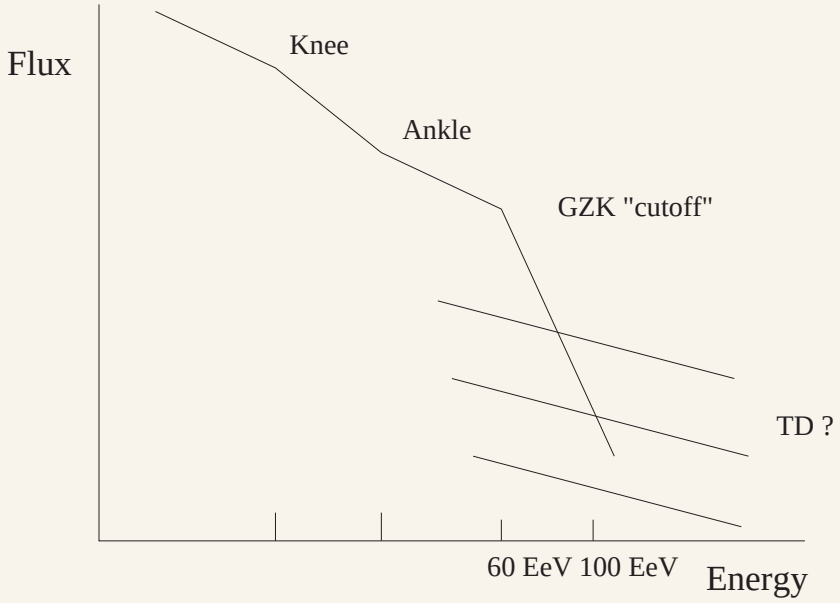

The MSRPs and certain classes of TDs may cluster in the Galactic Halo
$\Rightarrow$ Galactic T-D scenario $\rightarrow$
- Complete absence of GZK cutoff
- Anisotropy towards Galactic center

("unfavored"?).

More natural: Extragalactic T-D scenario (with Topological Defects) $\Rightarrow$ partial GZK cut-off followed by "recovery" (depends on the hardness of the spectrum). But strongly constrained by Extragalactic gamma ray background (EGRB).

Also, nearby, isolated, "bursting" T-D source of EHE particles possible — not constrained by EGRB.

- Topological Defects arise naturally in phase transitions associated with symmetry breaking
- TDs not "exotic" – routinely seen in lab systems
  – quantized flux tubes in type-II superconductors
  – vortex filaments in Liquid He
  – disclination lines in nematic liquid crystals
- Behavior of laboratory strings are well described by Kibble-Zurek theory initially developed in the context of cosmic strings.

“Strings” in Nematic Liquid Crystals

sure the plausible extrapolation of the reconstructed surface into unconstrained regions.
9. D. J. Struik, *Lectures on Classical Differential Geometry* (Dover, New York, ed. 2, 1988).
10. Estimates of nonshape parameters include an independent value for the rotation period ($P = 4.07 \pm 0.03$ hours) and refined values for the time delay τ and 2380-MHz Doppler frequency ν of hypothetical echoes from Castalia's central mass. Those values were received at the center of curvature of the Arecibo telescope's main reflector, at the epoch 22 August 1989 06:45:00 UTC: $\tau = 37,453,066.9 \pm 0.3$ μs and $\nu = 173,116.5 \pm 0.1$ Hz.
11. The Castalia data apparently require a waist with severe surface curvature. The rippled appearance of the low-g_{22} one-component models in Fig. 2A is an artifact, called Gibbs' phenomenon, of trying to use a truncated series to represent a sharply curving, nearly discontinuous function. The two-component model avoids this drawback.
12. Removing the "dynamical" penalty functions $A(\hat{p})$ and $B(\hat{p})$ and allowing the nominal model to reconverge decreased χ^2 by less than 0.1%.
13. For the nominal model, estimates of the scattering-law exponent and reflectivity (see Eq. 9) are $n = 2.8 \pm 0.3$ and $\rho = 0.80 \pm 0.03$, where the uncertainties encompass values for the upper and lower bound models. The most commonly used measure of a radar target's reflectivity is the radar albedo $\hat{\sigma} = \sigma/A_p$, which is the target's radar cross section divided by its projected area. Castalia's model albedo, averaged over all 64 frames, is 0.12 ± 0.01. A sphere with Castalia's values for ρ and n would have a radar albedo $\hat{\sigma} = 2\rho/(n + 1) = 0.16 \pm 0.01$; this "equivalent spherical albedo" may permit more useful comparisons with other radar targets.
14. M. J. S. Belton *et al.*, *Science* **257**, 1647 (1992).
15. P. C. Thomas, *Icarus* **77**, 248 (1989).
16. For a single-k observation, if k is replaced by $-k$ and the model is replaced by its mirror image through the equatorial plane, then $\sigma_{ij}(r, \varpi)$ is unchanged. The spin vector's sign (that is, the sense of rotation) and its azimuthal coordinate could have been constrained if other radar-target directions had been sampled.
17. This research was conducted at Washington State University and the Jet Propulsion Laboratory, California Institute of Technology, under contract with the National Aeronautics and Space Administration.

30 September 1993; accepted 6 January 1994

The Cosmological Kibble Mechanism in the Laboratory: String Formation in Liquid Crystals

Mark J. Bowick,* L. Chandar, E. A. Schiff, Ajit M. Srivastava

The production of strings (disclination lines and loops) has been observed by means of the Kibble mechanism of domain (bubble) formation in the isotropic-nematic phase transition of the uniaxial nematic liquid crystal 4-cyano-4′-*n*-pentylbiphenyl. The number of strings formed per bubble is about 0.6. This value is in reasonable agreement with a numerical simulation of the experiment in which the Kibble mechanism is used for the order parameter space of a uniaxial nematic liquid crystal.

Symmetry-breaking phase transitions in nature often spawn topological defects. An example of such defects from condensed matter physics is vortices produced when helium is cooled through its superfluid phase transition. An important proposal from cosmology is that the observed structure of the universe contains relics of topological defects formed as the early universe cooled. The important question of the density of defects was first treated theoretically by Kibble (*1*) using a model in which the phase transition proceeds by the formation of uncorrelated domains that subsequently coalesce, leaving behind defects. A domain is a uniform region of the ordered, or low-temperature, phase. Kibble assumed that the order varied randomly from one domain to the next and smoothly in between, and so proposed a straightforward statistical procedure for calculating the probability of string formation.

Although the Kibble mechanism was proposed for cosmic domains and strings, it should also describe the formation of strings or line defects in laboratory systems. Some time ago, Zurek (*2*) suggested the examination of vortex formation in liquid helium. The first experimental success, however, came in research by Chuang and co-workers (*3*, *4*). Working with nematic liquid crystals, these researchers were able to observe the evolution of line defects. In the present work, we report an experimental verification of a crucial aspect of the Kibble mechanism: String formation can be predicted statistically from domain coalescence. Experiments have also been reported recently on vortex line creation in liquid ^{3}He (*5*).

Nematic liquid crystals (NLCs) consist of rod-like molecules; the rods are randomly oriented in the isotropic, high-temperature phase but show long-range alignment in the nematic, orientationally ordered phase (*6*). To quantitatively distinguish the ordered and disordered phases, an order parameter is typically introduced. For NLCs, this parameter may be taken to be the mean orientation of rods. This value is zero in the isotropic phase and nonzero in the nematic phase. Orientational order in the nematic phase is described by a unit three vector $\mathbf{n}$ without sign, because there is no preferred polarity to the constituent rods ($\mathbf{n} \equiv \mathbf{n}$). Thus, the space of possible nematic ground states is the two-sphere S^2, with opposite points of the sphere regarded as the same (*7*). This space is rich in topological defects (*6*–*11*). It has point-like defects (monopoles), line defects (disclinations or strings), and three-dimensional defects (texture).

Before describing the present work with NLCs, we illustrate the Kibble mechanism using string formation for the simpler case of two spatial dimensions (planar spins) (*8*). The order parameter in some small spatial region is a unit vector with orientation θ varying between 0 and 2π (the ground-state manifold is a circle S^1). If we follow θ along a closed path, we can determine the total angle $\Delta\theta$ by which θ winds; of course $\Delta\theta$ must be some integer multiple of 2π. When $\Delta\theta$ is nonzero, a defect must be present inside the path (see Fig. 1A).

Consider now the situation when three randomly oriented domains meet at a point (Fig. 1B). We can then calculate the winding angle $\Delta\theta$ using a closed path that circulates in some specified direction around the intersection point; the dashed line in the figure illustrates such a path. If $\Delta\theta = +2\pi$, one type of elementary string is formed when the three domains coalesce.

The probability of string occurrence is

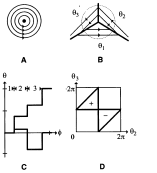

Fig. 1. A series of four diagrams illustrating the Kibble mechanism for planar spins. (**A**) The concentric circles indicate field lines of the order parameter and require an elementary topological defect at the origin. (**B**) Three domains with uniform order parameters θ_1, θ_2, and θ_3. The dashed circle indicates a loop around which a winding angle $\Delta\theta$ is calculated. (**C**) A graph illustrating the calculation of the winding angle for a path through three domains such as in (B). By definition, $\theta_1 = 0$. The jumps in θ between domains are minimized. This is the geodesic rule. Two different sets of order parameters are shown; the upper curve leads to defect formation ($\Delta\theta = +2\pi$), and the lower curve does not ($\Delta\theta = 0$). (**D**) The triangles labeled (+) and (−) indicate the combinations of θ_2 and θ_3 leading to $\Delta\theta = \pm 2\pi$ defects. One-fourth of all combinations lead to defect formation.

easily calculated. We denote the order parameters in the three domains as $\theta_1 = 0$, θ_2, and θ_3. We wish to calculate the winding angle $\Delta\theta$; the sequence of domains follows the circulation of our path. We also assume that the variation in θ from one domain to the next is minimized. For example, in Fig. 1C the upper curve has $\theta_3 > \pi$. We then show θ rising up to $+2\pi$ at the wall between domains 3 and 1. A return to $\theta = 0$ is excluded because this would require a larger jump. In fact, for a string in which $\Delta\theta = +2\pi$, we must have $\theta_3 > \pi$. We must also require $\theta_3 - \pi < \theta_2 < \pi$. If this second inequality is violated, we get $\Delta\theta = 0$ instead, as shown in the lower curve. Allowing windings by $\pm 2\pi$, one can readily estimate the probability P of forming a defect from the geometrical construction of Fig. 1D, obtaining $P = 1/4$ (*12*).

The generalization to three dimensions of the point defect just described for planar spins is a line defect. Spin systems, however, do not possess such line defects. Here the ground-state manifold is a sphere S^2; unlike the circle S^1, closed paths on a sphere are topologically equivalent to points and do not indicate line defects. Nematic liquid crystals, on the other hand, do exhibit line defects, because the orientation is described by a vector with the added property that orientations $\mathbf{n}$ and $-\mathbf{n}$ are equivalent [this ground-state manifold is denoted as the coset S^2/Z_2, where Z^2 is the cyclic group of order 2 $(1, -1)$] (*8*–*11*). A string defect in this case corresponds to the situation in which the director $\mathbf{n}$ rotates by π along a closed path; this is called a strength 1/2 defect. In two dimensions the Kibble prediction for the probability of defect formation for the manifold S^1/Z_2 can again be obtained analytically, yielding $1/\pi$ (*13*).

We now turn to our experiments and simulations. We studied the NLC K15 (4-cyano-4′-*n*-pentylbiphenyl; BDH Chemicals, Ontario). We used an Olympus model BH phase-contrast microscope, equipped with a monochrome television camera and a standard video cassette recorder. We placed a drop of K15 on a clean, untreated microscope slide and heated the drop with an illuminator. After a slow reduction of intensity, we were able to obtain clear images of bubble formation and evolution as the drop cooled through the isotropic-nematic (I-N) phase transition at 35.3°C.

One set of such images is reproduced in Fig. 2. Figure 2A shows the numerous small isolated bubbles of the nematic phase that form first. At short intervals later, the nematic bubbles increase in size (Fig. 2, B and C), both by natural growth and by coalescence. In the next stage, the organization of the NLC into bubbles is replaced by an image of a homogeneous medium with entangled strings (Fig. 2D), which further evolve by straightening, shrinking, and the excision of small loops of closed string (Fig. 2E). The associated string dynamics have been well described (*3*, *4*). As time passes, the string pattern “coarsens.”

An important aspect of these observations is that the nematic bubbles shown in Figs. 2, A to C, formed in a single sheet near the top of the liquid crystal droplet. The depth of field of our microscope was about 40 μm. We see no out of focus bubbles, nor do we see the shadowing of bubbles by other bubbles. We presume that the liquid crystal cooled most rapidly near the air interface, leading to the formation of a nematic sheet at this interface.

It is fairly straightforward in the examination of Fig. 2C to select a minimal, spherical bubble that may contribute to the observed string formation. Larger, oddly shaped bubbles arise from the coalescence of two or more minimal bubbles. We therefore estimate the total number of bubbles N for the image by counting the total number of minimal bubbles involved, with coalesced bubbles counted as the appropriate multiple. In Fig. 2C we find $N \sim 55$. This procedure is somewhat ambiguous, and we found about a 10% standard deviation in independent estimates of the bubble count in a given picture. This value is compatible with the standard deviation in the bubble count for different sequences.

We now proceed to estimate the expected number of strings per bubble n_1 from the measured string length L_s in Fig. 2D and the bubble count N. The total string length is $L_s = n_1 N d$, where d is the linear size of a minimal bubble. This size may be estimated as $d = \sqrt{A/N}$, where A is the area of the image in Fig. 2C. Thus, we find $n_1 = L_s/\sqrt{AN}$. For Fig. 2C we measure $L_s \simeq 2.7$ mm, yielding $n_1 \sim 0.61$. We repeated this analysis on three sequences, obtaining $n_1 = 0.64 \pm 0.02$ for the average number of strings per bubble. The error here is the simple statistical error in the mean. Our true errors are dominated by the ambiguities in bubble count mentioned above and by the coarsening of strings between Figs. 2C and 2D, which reduces the string length.

We now estimate the probability of string formation in our experiment using an elaboration of the Kibble calculation described earlier. For this estimation, we need a model for the directors in a “raft” of nematic bubbles just before coalescence (Fig. 2C). We assume that the director orientation inside a given bubble is roughly uniform and that this overall orientation varies randomly from one bubble to another. The top portions of the bubbles are in contact with air. We also assume that the

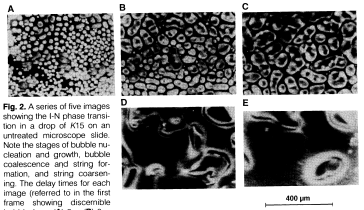

Fig. 2. A series of five images showing the I-N phase transition in a drop of K15 on an untreated microscope slide. Note the stages of bubble nucleation and growth, bubble coalescence and string formation, and string coarsening. The delay times for each image (referred to in the first frame showing discernible bubbles) are (**A**) 2 s, (**B**) 3 s, (**C**) 5 s, (**D**) 11 s, and (**E**) 23 s. The scale is for all five pictures.

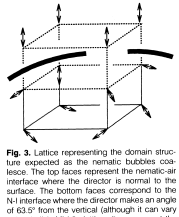

Fig. 3. Lattice representing the domain structure expected as the nematic bubbles coalesce. The top faces represent the nematic-air interface where the director makes an angle of 63.5° from the vertical (although it can vary azimuthally). Middle lattice sites represent the regions near the centers of the bubbles.

M. J. Bowick, L. Chandar, E. A. Schiff, Department of Physics, Syracuse University, Syracuse, NY 13244–1130, USA.
A. M. Srivastava, Institute for Theoretical Physics, University of California, Santa Barbara, CA 93106, USA.
*To whom correspondence should be addressed.

General Characteristics of T-D models of EHE particle production

X particle decay: Likely to involve new physics (e.g., SUSY ?)

$$X \rightarrow q\,,\ell\,,\ldots \text{new particles}$$

$$q \rightarrow N\,,\pi\,,K\,,\ (\text{parton shower and fragmentation})$$

Parton Shower

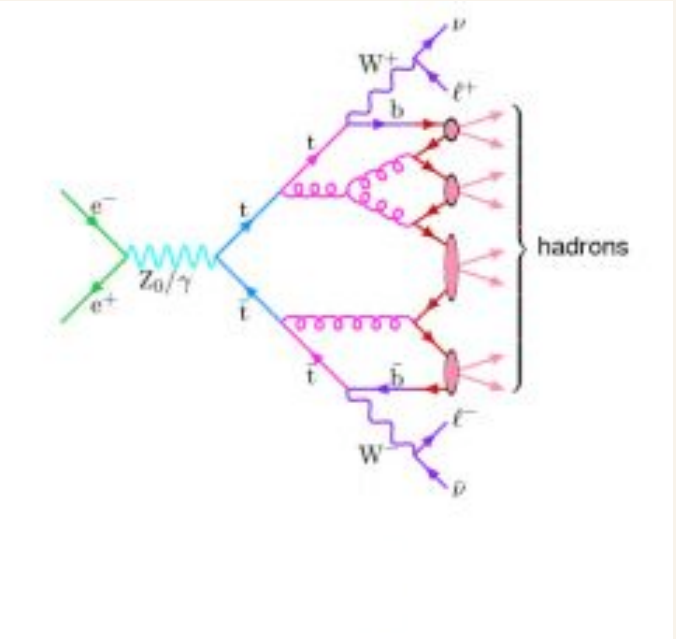

$$N/\pi \lesssim 10\%\,, \;\; \pi \to e^{\pm}\,, \gamma\,, \nu\,(+\bar{\nu})$$

Final hadron energy spectra are determined by Fragmentation Functions (FFs): $F^h(x, s = M_X^2)$

$$\frac{dN^h}{dx}(x,s) \equiv F^h(x,s) \propto \Sigma_a \int_x^1 \frac{dz}{z} \frac{d\Gamma_{X\to a}}{dz}(z,s) D_a^h(x/z,s)\,,$$

$d\Gamma_{X\to a}/dz =$ decay width of the X into parton a: Calculable in perturbation theory

D_a^h is the perturbatively non-calculable parton-to-hadron fragmentation function.
But evolution of D_a^h's in s can (in principle) be calculated in perturbation theory: DGLAP eqn. in QCD.

$D_a^h(x,s)$ can be experimentally determined at low s from say, $e^+e^- \to \gamma/Z \to q\bar{q} \to h + \cdots$. Can then evolve them to get the FFs at any s. (but ?)

Coherent branching in parton shower + "Local Parton-Hadron Duality": An analytical approach
Color coherence $\longrightarrow$ angular ordering of the parton shower development $\longrightarrow$ Modified "DGLAP" eqn.

To leading order, the singlet FF $D_S^h \equiv \Sigma_a D_a^h(x,s)$ is a Gaussian in $\xi \equiv \ln(1/x)$

$$D_S(\xi) \equiv x D_S(x,s) \propto \exp\left[-\frac{1}{2\sigma^2}\left(\xi - \xi_p\right)^2\right],$$

where the peak position $\xi_p = Y/2$, and $2\sigma^2 = (bY^3/36N_c)^{1/2}$, with $Y \equiv \ln(M_X/\Lambda_{\rm eff})$ and $b = (11N_c - 2n_F)/3$, $N_c = 3 =$ number of colors, $n_F =$ number of flavors.

Higher order $\longrightarrow$ MLLA $\longrightarrow$ "distorted Gaussian"

QCD DGLAP evolution of FF

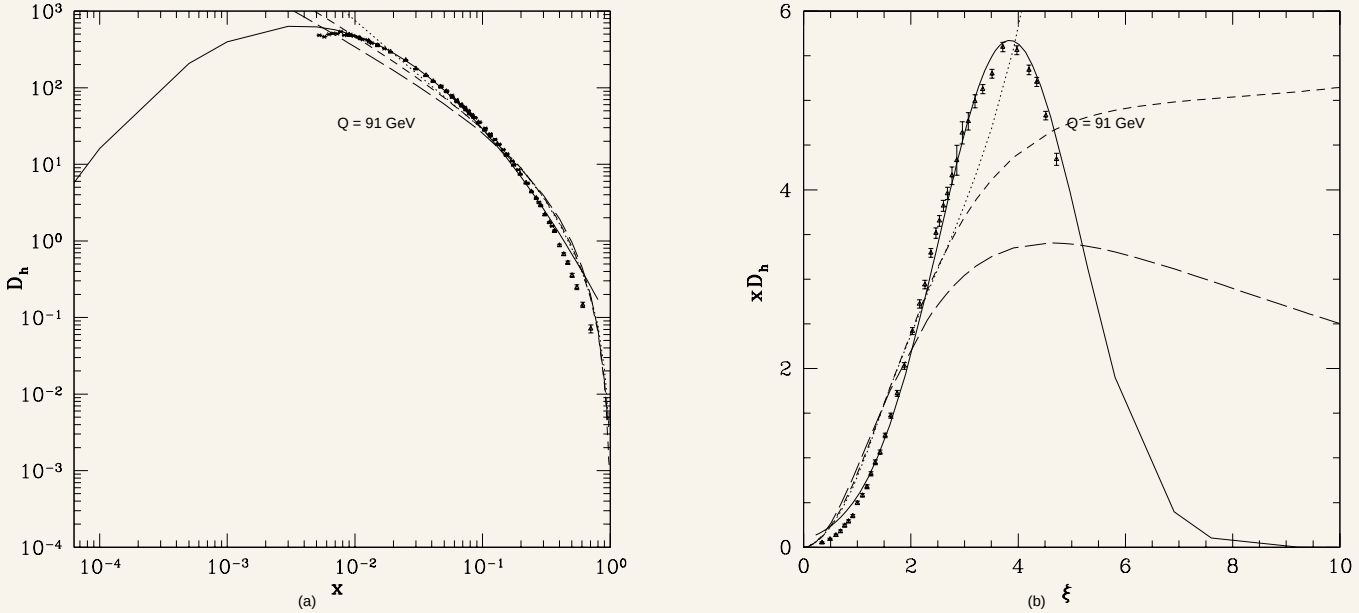

solid curve: "Gaussian";
Numerical DGLAP evolution with parametrized initial FFs —
dotted: KKP; short-dashed: BKK; long-dashed: Kretzer

(From R. Basu and P. Bhattacharjee, PRD 70 (2004) 023510)

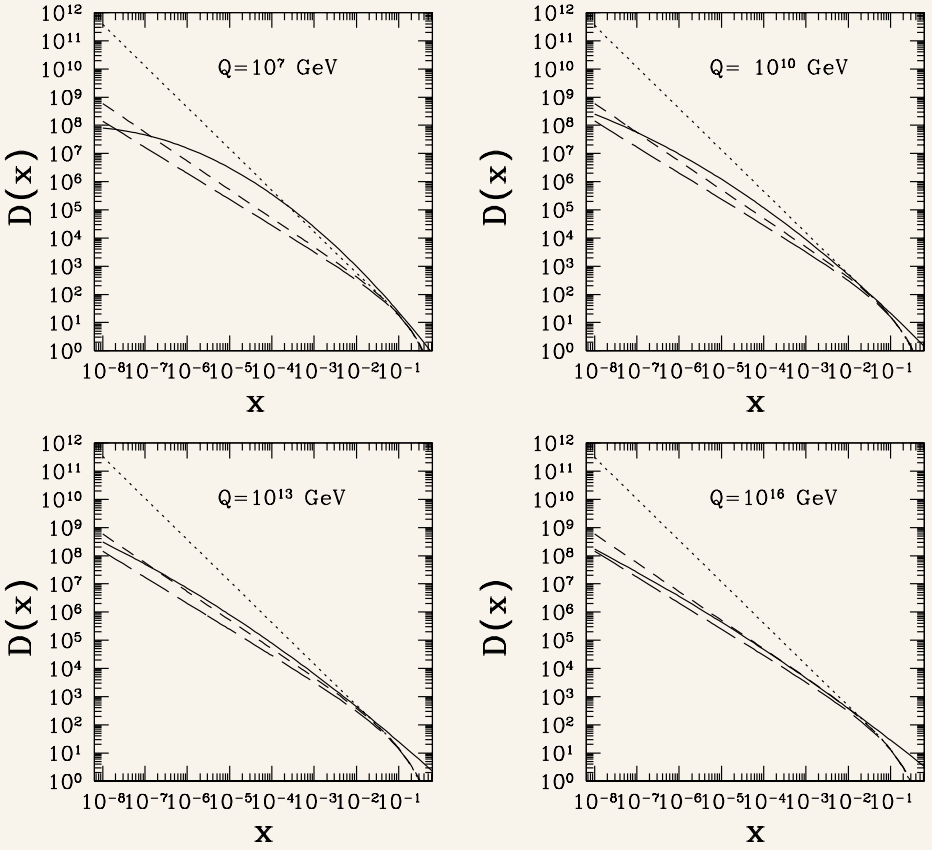

(From R. Basu and P. Bhattacharjee, PRD 70 (2004) 023510)

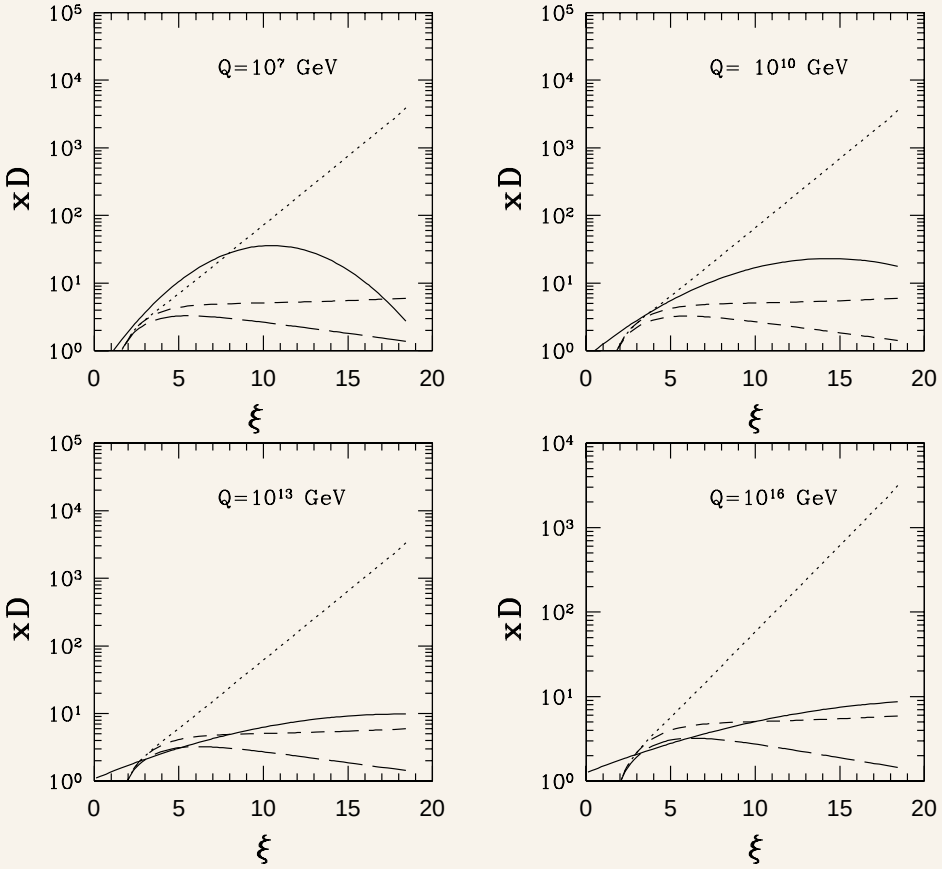

(From R. Basu and P. Bhattacharjee, PRD 70 (2004) 023510)

- Numerical evolution of DGLAP with SUSY
- Direct numerical simulation of parton shower and hadronization

. . .

Sarkar & Toldra, Rubin, Barbot & Drees, Aloiso, Berezinsky, Kachelriess, Fodor & Katz,

. . .

- Many uncertainties . . .

The simple "Gaussian" is good enough for now for most practical purposes!

Injection spectra of particles in T-D scenario

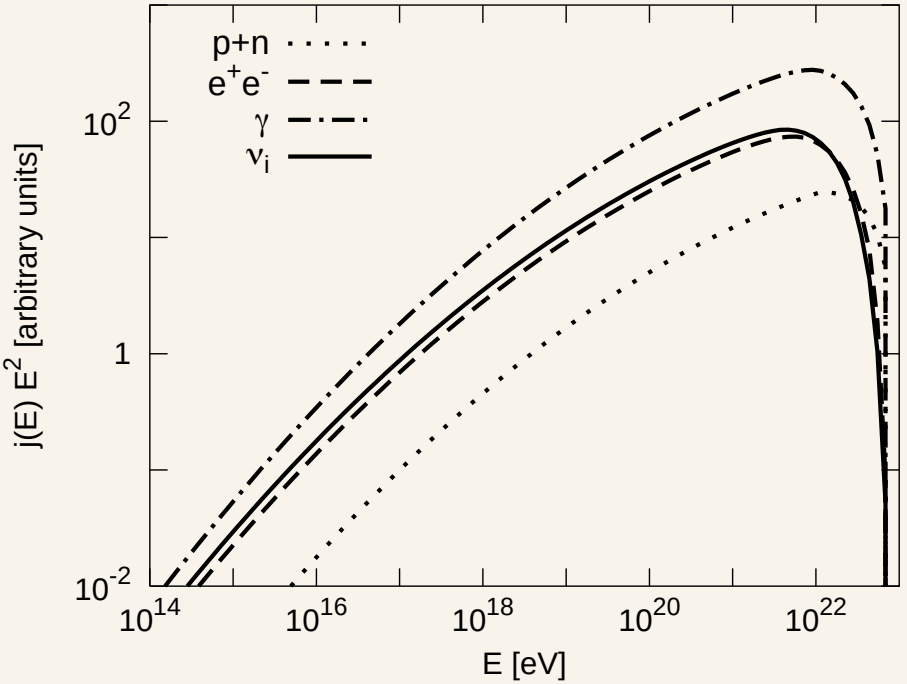

(From Kalashev et al, PRD 66 (2002) 063004)

Benchmark requirements and constraints on T-D models of EHECR

Consider $X \to q\bar{q} \to$ hadrons with

$$\pi^0 \to 2\gamma\,,\ \pi^+ \to e^+\nu_e\nu_\mu\bar{\nu}_\mu\,,\ \pi^- \to e^-\bar{\nu}_e\nu_\mu\bar{\nu}_\mu\,,$$

(Assume equal energy sharing by individual particles)

For every E_π, get $E_{\rm em} : E_{\nu_\mu} : E_{\nu_e} \approx \frac{1}{2} : \frac{1}{3} : \frac{1}{6}$

Assume a power-law spectrum with index α:

$$dN_\gamma/dE_\gamma \approx 1.8(2-\alpha)(f_\pi/0.9)M_X^{-1}(2E_\gamma/M_X)^{-\alpha}$$

Assuming uniform distribution:

$$j_\gamma(E_\gamma) \simeq \frac{1}{4\pi} l(E_\gamma)\,\dot{n}_X\,\frac{dN_\gamma}{dE_\gamma}$$

Normalizing to a fiducial EHECR flux, we get

$$(\dot{n}_{X,0})_{\rm EHECR} \simeq 1.3\times10^{-45}\,{\rm cm^{-3}\,s^{-1}}\left(\frac{l(E_\gamma)}{10\,{\rm Mpc}}\right)^{-1}\left(\frac{E^2 j(E)}{1\,{\rm eV\,cm^{-2}\,sec^{-1}\,sr^{-1}}}\right)\left(\frac{E}{10^{11}\,{\rm GeV}}\right)^{\alpha-2}$$
$$\times\left(\frac{m_X}{10^{13}\,{\rm GeV}}\right)^{1-\alpha}\left(\frac{0.5}{2-\alpha}\right)\left(\frac{0.9}{f_\pi}\right)2^{(\alpha-1.5)}10^{(3-2\alpha)}\,.$$

Required injection rate

$$(\dot{n}_{X,0})_{\rm EHECR} \sim 1.1\times 10^{36}\,{\rm Mpc}^{-3}\,{\rm yr}^{-1}\left(\frac{l(E_\gamma)}{10\,{\rm Mpc}}\right)^{-1}\left(\frac{m_X}{10^{13}\,{\rm GeV}}\right)^{1-\alpha}$$

$$(Q_{X,0})_{\rm EHECR} \sim 1.3\times 10^{-23}\,{\rm eV\,cm}^{-3}\,{\rm s}^{-1}\left(\frac{l(E_\gamma)}{10\,{\rm Mpc}}\right)^{-1}\left(\frac{m_X}{10^{13}\,{\rm GeV}}\right)^{2-\alpha}$$

$$(Q_{X,0})_{\rm EHECR} \sim 1.7\times 10^{46}\,{\rm erg\,Mpc}^{-3}\,{\rm yr}^{-1}\left(\frac{l(E_\gamma)}{10\,{\rm Mpc}}\right)^{-1}\left(\frac{m_X}{10^{13}\,{\rm GeV}}\right)^{2-\alpha}$$

Electromagnetic cascade due to UHE γ injection

- EM energy injected above $\sim 10^{15}\,{\rm eV}/(1+z)$ cascades down to below 100 GeV due to $\gamma\gamma_b \to e^+e^-$ and $e\gamma_b \to e\gamma$.
- Measured Extragalactic Gamma Ray Background (EGRB) in the (10 MeV – 100 GeV) region (EGRET) puts constraints on allowed EM energy injection at UHE above the pair production threshold on CMB/Radio background target photons.

$$w_{\rm cascade} \sim fQ_X t_0 \approx f\times 3.9\times 10^{-6}\,{\rm eV\,cm}^{-3}$$

Require $w_{\rm cascade} < w_{\rm EGRB} \sim (3-6)\times 10^{-6}\,{\rm eV\,cm}^{-3}$. Not easy!

Propagation of EHE particles

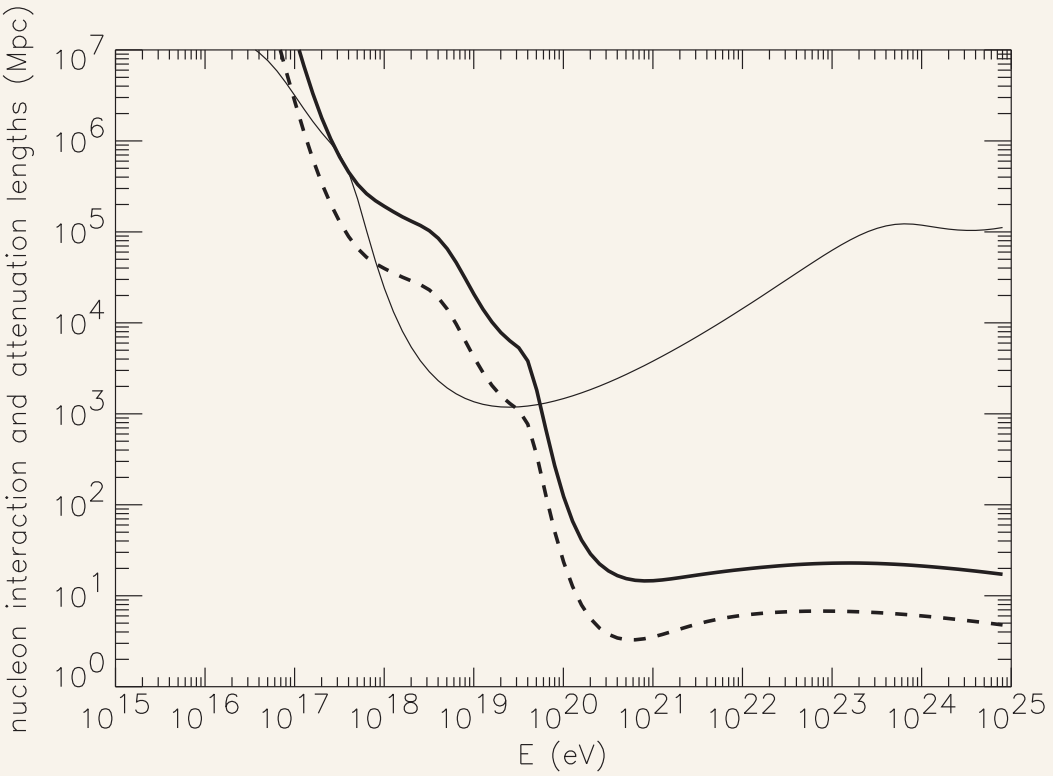

Thick solid line: Att. length for $N\gamma \longrightarrow N\pi$
Thick dashed line: Int. length for $N\gamma \longrightarrow N\pi$
Thin solid line: Att. length for $p\gamma \longrightarrow e^+e^-p$
(From Bhattacharjee & Sigl: Phys. Rep. (2000).)

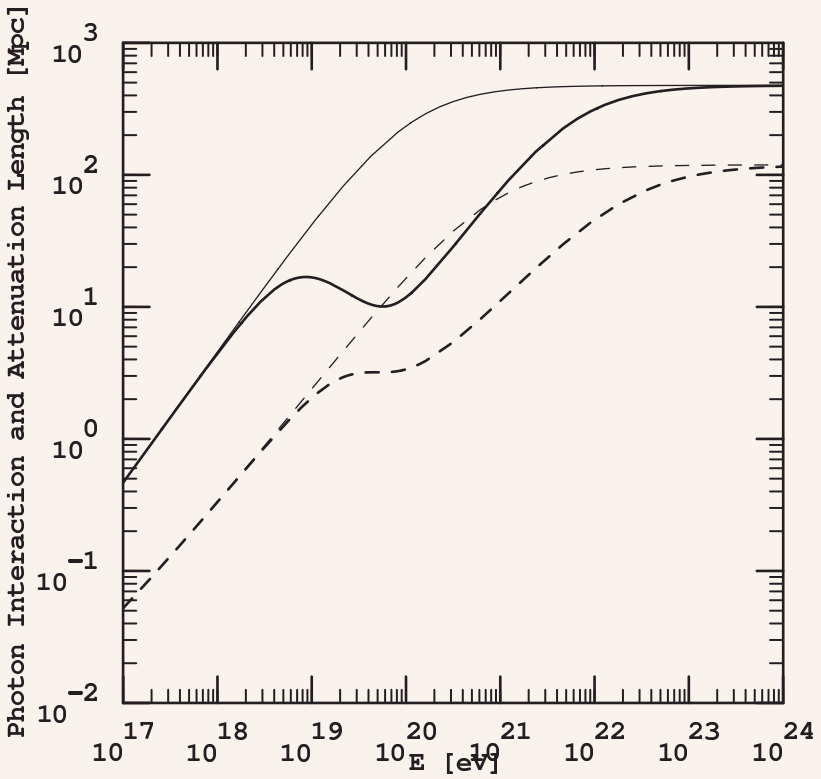

$\gamma\gamma \longrightarrow e^+e^-$

Solid: Att. length; dashed: Int. length

Thick: In CMB + Radio; Thin: In CMB only.

(From Bhattacharjee & Sigl: Phys. Rep. (2000).)

EHE Particle Fluxes in the Extragalactic TD Scenario

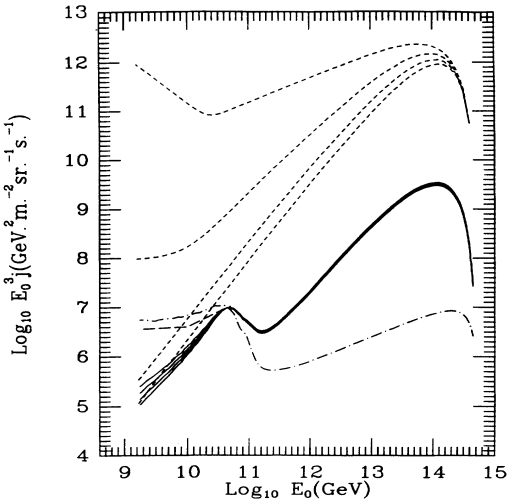

FIG. 1. The UHE proton spectrum due to topological defects, for $m_X = 10^{15}$ GeV. The four solid curves (which are indistinguishable for $E_0 > 5\times10^{10}$ GeV) are the *maximal* flux spectra for $p = 1.5$, 1, 0.5, and 0, respectively (from bottom to top), the corresponding values of $\kappa_{\max}$ being 1.18×10^{-29}, 0.2313, 4.52×10^{27}, and 8.82×10^{55}, respectively. The four short-dashed curves ("redshifted injection spectra") correspond to the same four values and order of p and corresponding $\kappa_{\max}$ as above, but calculated without considering any energy loss of protons *except* that due to expansion of the Universe. The dashed curve (terminating at 7×10^{10} GeV) represents the UHE CR flux given by the Fly's Eye group [15], and the dash-dotted curve immediately above it is for an injection spectrum $\propto E_i^{-2.5}$. The normalization of the last curve has been conveniently chosen for clarity.

(From Bhattacharjee, Hill, Schramm: PRL 69 (1992) 567)

Photon/Proton Ratio: A Signature of TD Scenario

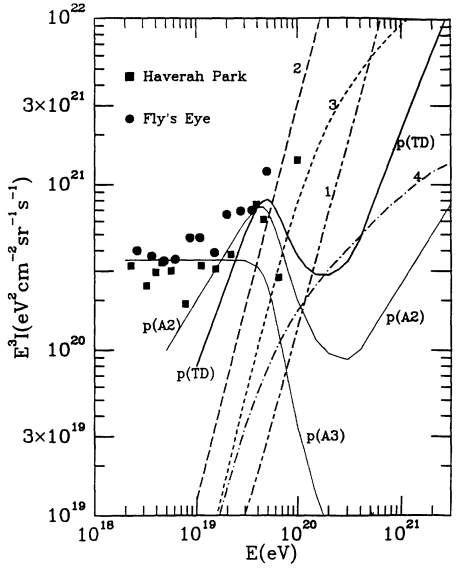

FIG. 1. Equilibrium spectra of protons and γ rays. The curves p(A2) and p(A3) are the proton spectra in the A model with $\alpha=2$ and 3, respectively. The curve marked p(TD) is the proton spectrum in the TD model. The curves 1,2,3,4, are equilibrium γ-ray spectra calculated for TD model: (1) direct γ rays; (2) cascade γ rays neglecting interactions with the intergalactic magnetic field ($B \ll 10^{-12}$ G) and universal radio background ($w_{\rm URB} \ll w_r$); (3) cascade γ rays with $w_{\rm URB}=w_R$, $B=3\times10^{-11}$ G; (4) same as (3) with $B=10^{-10}$ G.

(From Aharonian, Bhattacharjee, Schramm: PRD 46 (1992) 4188)

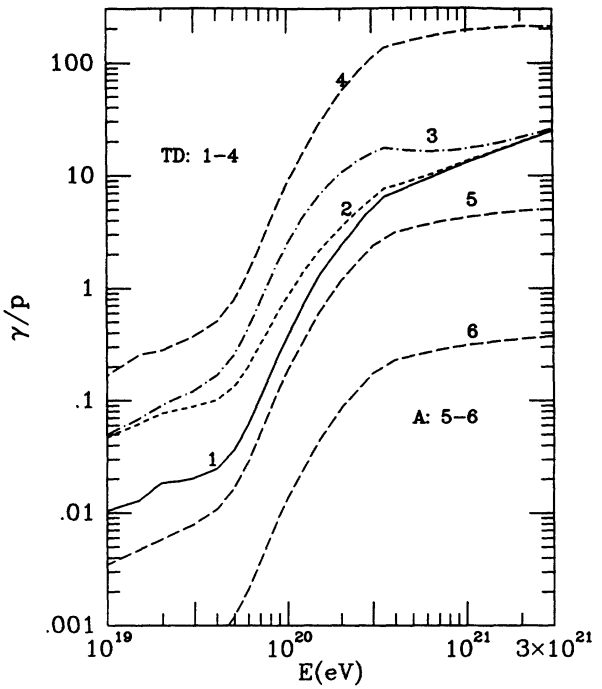

FIG. 3. The γ/p ratio expected in the TD and A models. The curves marked 1, 2, 3, and 4 are for the TD model. The curves 5 and 6 are for the A model with $\alpha=2$ and 3, respectively. (1) Direct γ rays; (2) cascade γ rays with $w_{\rm URB}=w_R$ and $B=10^{-10}$ G; (3) same as (2) except $B=3\times10^{-11}$ G. The curves 4, 5, and 6 are for $w_{\rm URB}\ll w_R$ and $B<10^{-12}$ G.

(From Aharonian, Bhattacharjee, Schramm: PRD 46 (1992) 4188)

Particle Fluxes vs. EGRET γ-Ray Background Flux

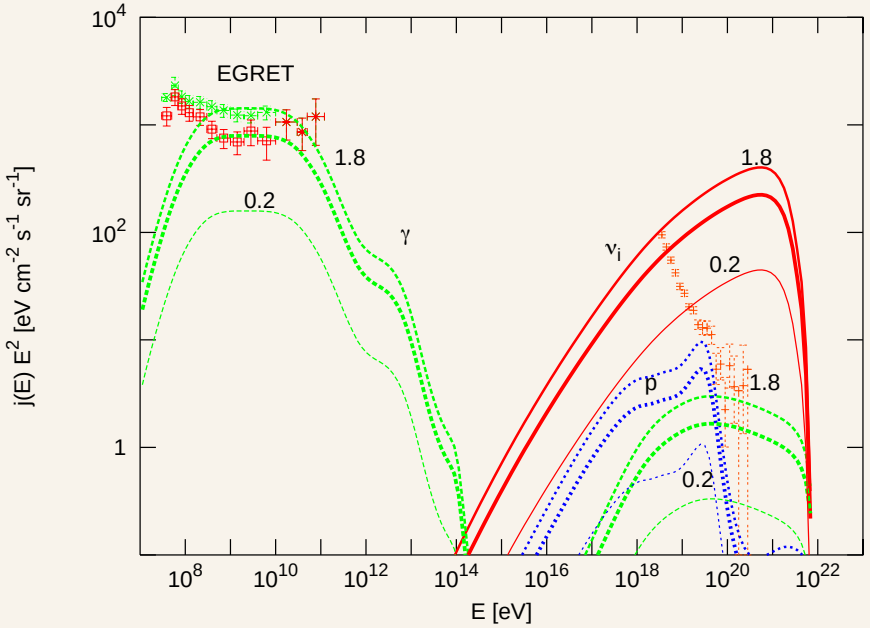

(From Semikoz & Sigl, JCAP 0404, 003 (2004), hep-ph/0309328)

Assumed uniformly distributed extragalactic TD sources with $\dot{n_X} \propto t^{-3}$ (e.g., collapsing cosmic string loops) with $m_X = 2 \times 10^{13}\,\mathrm{GeV}$, $B = 10^{-12}\,\mathrm{G}$.

Neutrino Fluxes

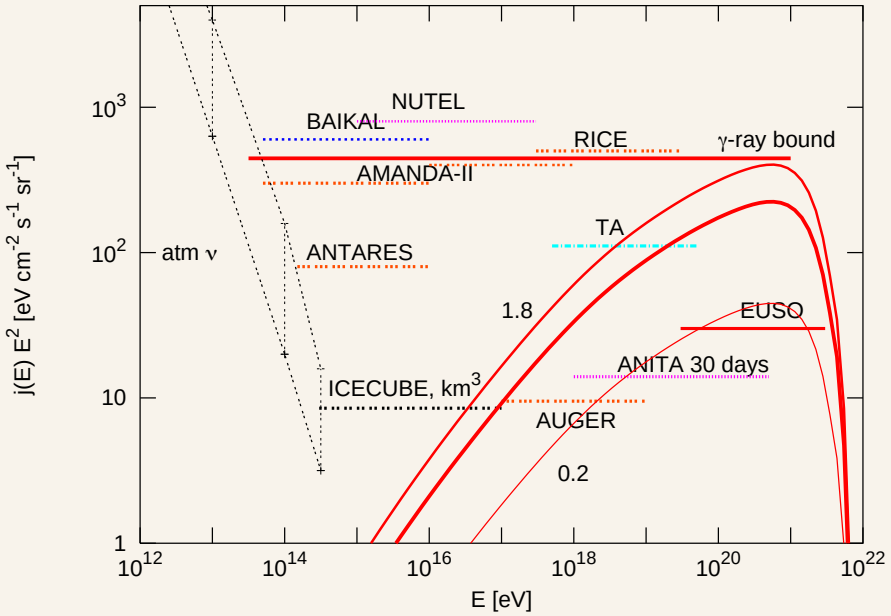

(From Semikoz & Sigl, JCAP 0404, 003 (2004), hep-ph/0309328)

Assumed uniformly distributed extragalactic TD sources with $n_X \propto t^{-3}$ (e.g., collapsing cosmic string loops) and $m_X = 2 \times 10^{13}\,\mathrm{GeV}$, $B = 10^{-12}\,\mathrm{G}$.

Example of possible T-D sources: Cosmic String

- Cosmic strings are expected in any $U(1)$-symmetry breaking phase transition
- Closed loops of cosmic strings form due to self-intersections of the string $\longrightarrow$ scaling of the string network
- Some closed loops collapse or repeatedly self-intersect and disappear into massive X particles (massive gauge bosons, higgs bosons) of the broken $U(1)$ (PB, Kibble, Turok 1982; PB and Rana 1990; Siemens and Kibble 1994)
- X particles may also be directly emitted from strings (Vincent, Antunes, Hindmarsh 1998)

In general, for processes involving scaling TDs,

$$\dot{n}_X(t) = (Q_0/M_X)(t/t_0)^{-4+p}$$

(PB, Hill, Schramm, PRL 1992).

- For rapidly collapsing cosmic strings $p = 1$.

Cosmic strings are expected in Baryogenesis via Leptogenesis scenario of generating the Baryon asymmetry of the Universe due to breaking of the $U(1)_{B-L}$.

Cosmic String

$\mathcal{L} = -\frac{1}{4}F_{\mu\nu}F^{\mu\nu} + (D_\mu\phi^*)(D^\mu\phi) - V(\phi)\,,$

$D_\mu\phi = (\partial_\mu - ieA_\mu)\phi\,,\ F_{\mu\nu} = (\partial_\mu A_\nu - \partial_\nu A_\mu)\,,$

$V(\phi) = \frac{1}{4}\lambda(\phi^*\phi - \eta^2)^2\,.$

- The $U(1)$ symmetry $\phi \longrightarrow e^{i\alpha}\phi$ is spontaneously broken.
- No unique ground state: A continuous manifold (circle) of degenerate ground states $\phi = \eta e^{i\theta}$.
- Vortex String allowed since $\Pi_1(S^1) \neq 1\,.$

Cosmic String

$\mathcal{L} = -\frac{1}{4}F_{\mu\nu}F^{\mu\nu} + (D_\mu\phi^*)(D^\mu\phi) - V(\phi)\,,$
$D_\mu\phi = (\partial_\mu - ieA_\mu)\phi\,,\ F_{\mu\nu} = (\partial_\mu A_\nu - \partial_\nu A_\mu)\,,$
$V(\phi) = \frac{1}{4}\lambda(\phi^*\phi - \eta^2)^2\,.$

- The $U(1)$ symmetry $\phi \longrightarrow e^{i\alpha}\phi$ is spontaneously broken.
- No unique ground state: A continuous manifold (circle) of degenerate ground states $\phi = \eta e^{i\theta}$.
- Vortex String allowed since $\Pi_1(S^1) \neq 1\,.$

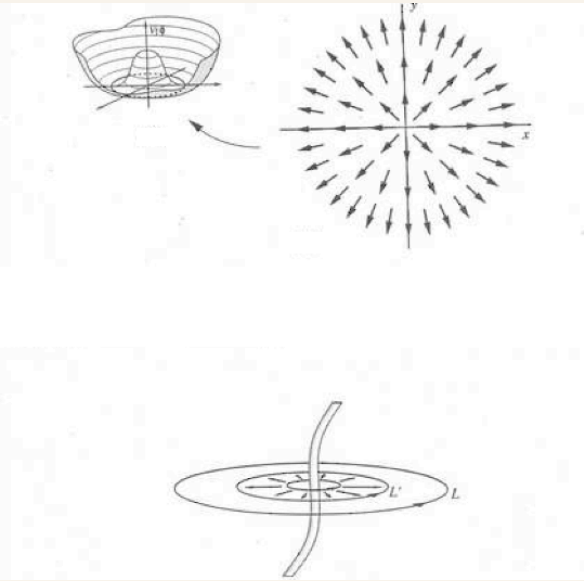

$\phi = f(r)\eta e^{in\theta}\,,\quad A_\mu = \frac{ng(r)}{er}\delta^\theta_\mu\,,$
$r = \sqrt{(x^2+y^2)}\,,\quad n = \text{integer}$
$f(r) \sim e^{-rm_\phi}\,,\quad g(r) \sim e^{-rm_V}$
$f(0) = g(0) = 0\,,\quad f(\infty) = g(\infty) = 1$
Energy per unit length, $\mu \approx \eta^2 = 9 \times 10^{21}\,\mathrm{g/\,cm}(\eta/10^{16}\,\mathrm{GeV})^2$
$G\mu = 6.7 \times 10^{-7}(\eta/10^{16}\,\mathrm{GeV})^2$

Kibble mechanism of cosmic string formation

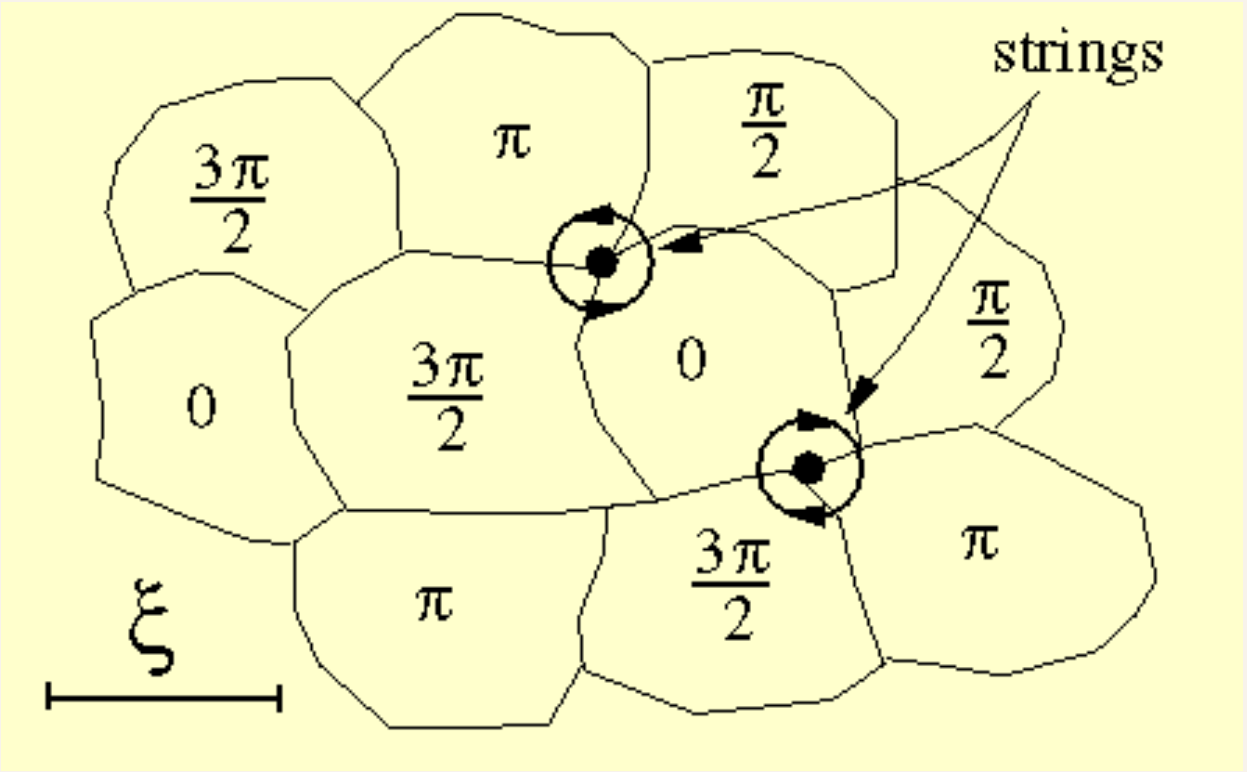

Evolution of cosmic string network: Numerical simulation

Radiation era

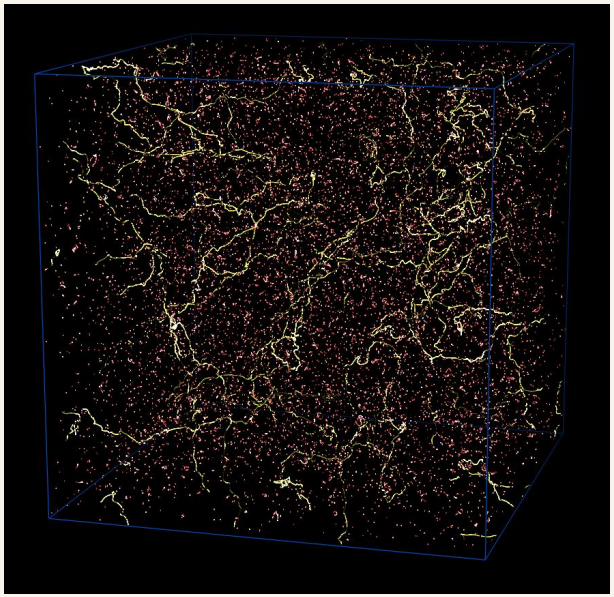

Matter era

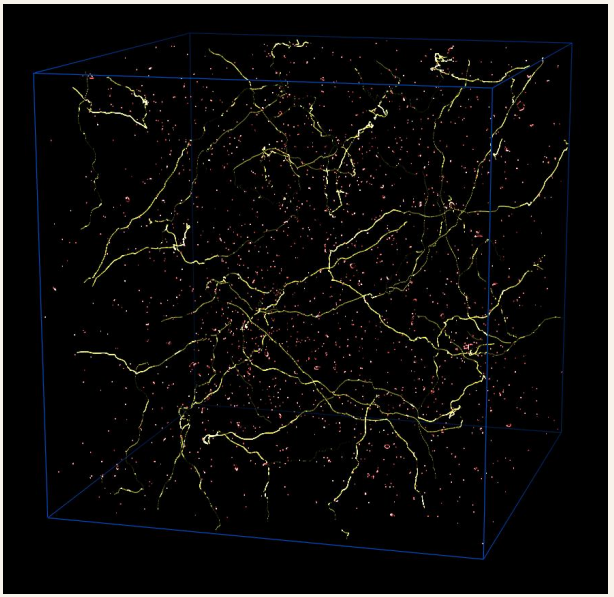

(From simulations by Paul Shellard)

Loop production and scaling

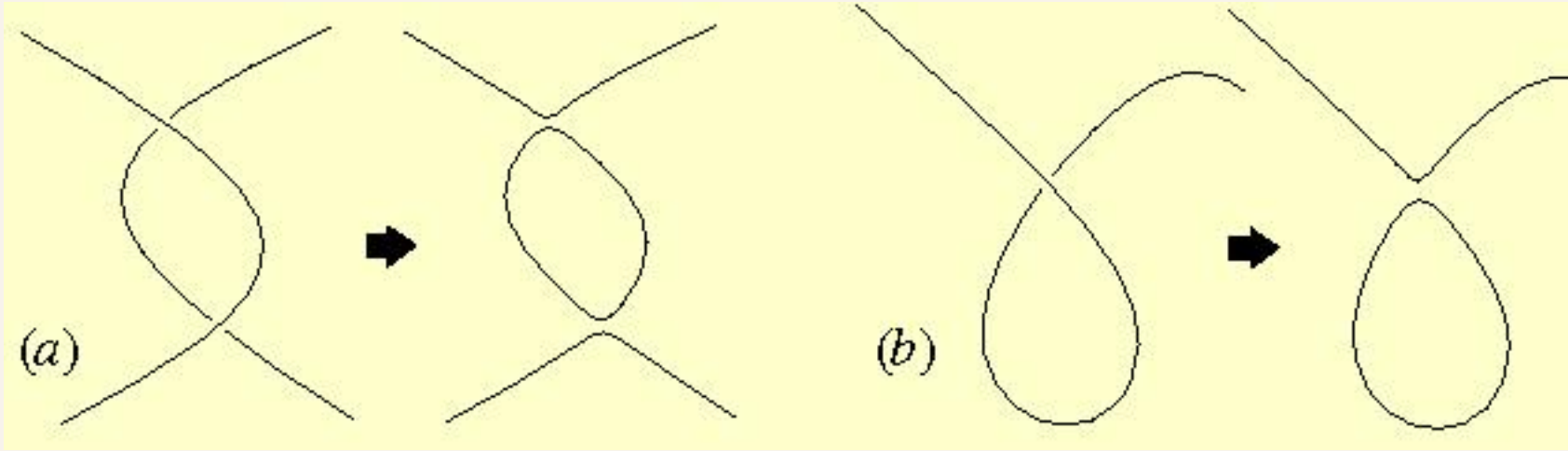

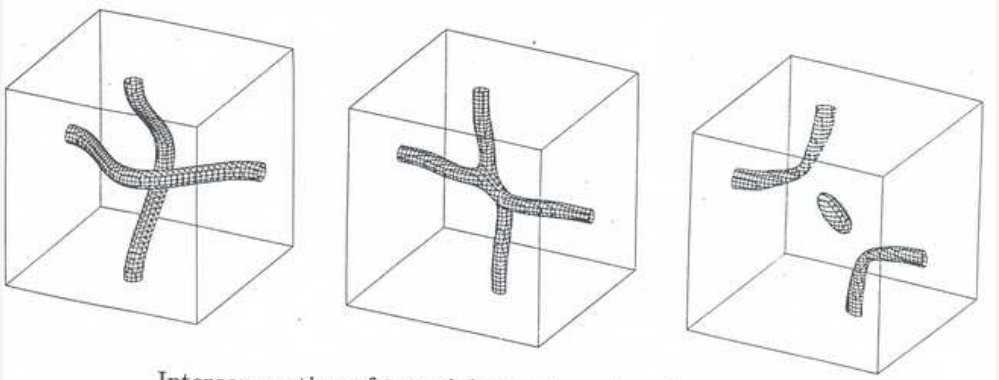

Intercommuting of two global strings. In this energetic intersection, the creation of an 'interaction loop' can be observed in the aftermath [Shellard, 1992].

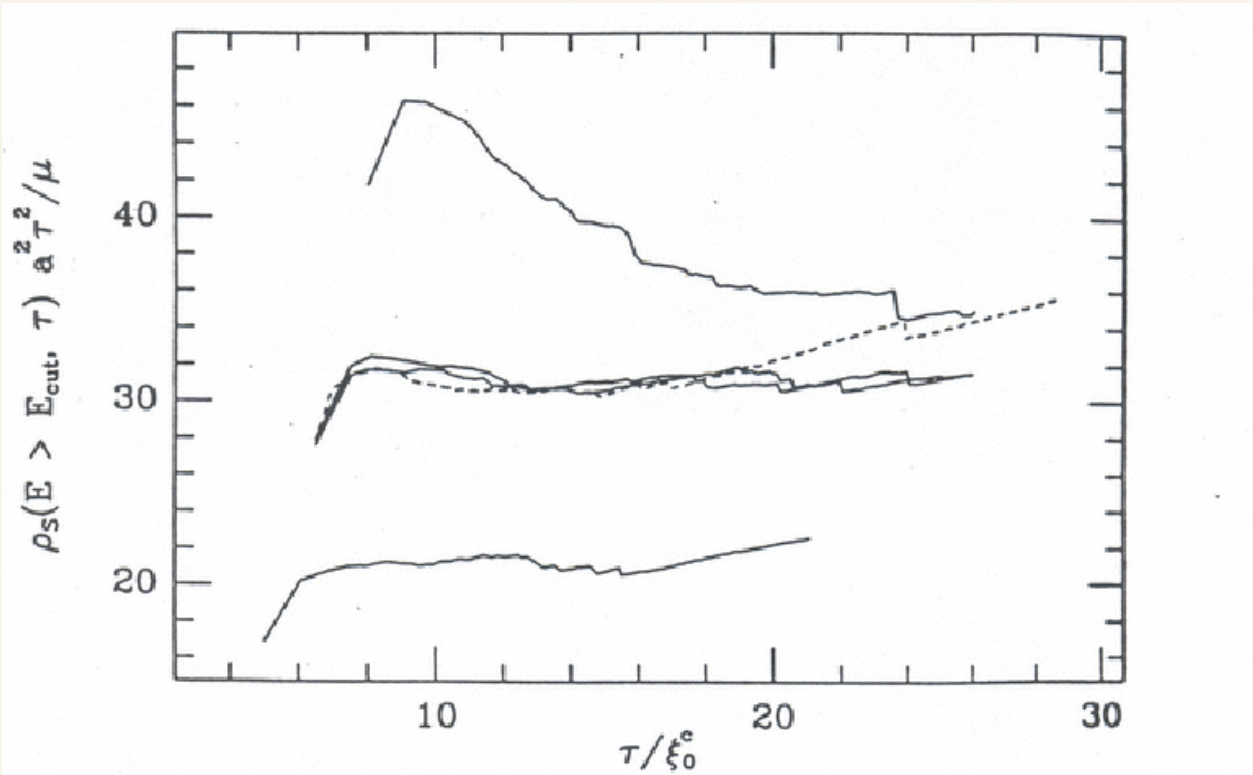

Approach to scaling in the matter era [Bennett & Bouchet, 1990].

Loop formation rate

To maintain scaling, closed loops of average length $L_b = K\Gamma G\mu t$ are formed at a rate (in matter era)

$$\frac{dn_b}{dt} = \frac{2}{3x^2}\,(\Gamma G\mu)^{-1} K^{-1} t^{-4}\,.$$

$(x \simeq 0.3\,,\ \Gamma \simeq 100\,,\ K \sim O(1)\,..$

Loops oscillate and lose energy slowly by emitting gravitational radiation at a rate $\dot{E}_{\rm grav} = \Gamma G\mu^2$. So, a loop of length L has a (gravitational radiation) lifetime $\tau_{\rm grav} = (\Gamma G\mu)^{-1} L$.

The most abundant loops today have

- Typical length: $\sim 0.2(G\mu/10^{-12})(\Omega_0 h^2)^{-1/2}\,{\rm pc}$
- Number density: $\sim 4.6(G\mu/10^{-12})^{-1}(\Omega_0 h^2)^{3/2}\,{\rm Mpc}^{-3}$
- Typical separation between loops: $\sim 600(G\mu/10^{-12})^{1/3}(\Omega_0 h^2)^{-1/2}\,{\rm kpc}$.

(Note: $G\mu \simeq 10^{-12}$ for $\eta \sim M_X \sim 10^{13}\,{\rm GeV}$.)

Quick death of loops

A small fraction of loops my die quickly on time scales $\ll$ Hubble time.

Self-intersection probability of a loop is $P_{SI} \simeq 1 - e^{-\alpha-\beta N}$, $N =$ number of harmonics on the loop. (Siemens and Kibble 1994).

So, very "kinky" (large N) loop of length L will self-intersect on a time scale $\sim L/2$ and break into two daughter loops. Since intersection leaves behind further kinks, the daughter loops will further break into grand-daughter loops on time scale $\sim L/4$ and so on.

Thus a single loop of initial length L can break up into a debris of tiny loops of length $\sim \eta^{-1}$ (they then become X particles) on a time scale $\tau_{\rm collapse} \sim L \ll t$.

A typical loop of length $\sim 0.2\,{\rm pc}$ will collapse over a period $\sim 0.6\,{\rm yr}$ releasing a total energy $\sim (G\mu/10^{-12})4.4 \times 10^{54}\,{\rm erg}$.

(A "bursting" T-D source!)

$\dot{n}_X^{\rm QD} = f_{\rm QD}\frac{1}{x^2}\mu^{1/2}t^{-3}$ with $f_{\rm QD} < 1$.

Conclusions

- New physics beyond SM based on unified symmetry and symmetry breaking generically lead to formation of Topological Defects.
- Under many circumstances TDs may collapse, releasing their energy into massive particles with $M_X > 10^{12}\,\mathrm{GeV}$. Their decay can give rise to EHE particles.
- Generally predict hard, γ and ν dominated spectra.
- Can these particles be detected against "background" from astrophysical sources ?